nature physics

LETTERS

https://doi.org/10.1038/s41567-021-01501-y

Check for updates

OPEN

Robustness of the thermal Hall effect close to half-quantization in α-$RuCl_3$

J. A. N. Bruin[1]✉, R. R. Claus[1], Y. Matsumoto[1], N. Kurita[2], H. Tanaka[2] and H. Takagi[1,3]✉

A key feature of quantum spin liquids is the predicted formation of fractionalized excitations. They are expected to produce changes in the physical response, providing a way to observe the quantum spin liquid state[1]. In the honeycomb magnet α-$RuCl_3$, a quantum spin liquid has been proposed to explain the behaviour observed on applying an in-plane magnetic field $H_{||}$. Previous work reported that the thermal Hall conductivity took on a half-integer quantized value and suggested this as a signature of a fractionalized Majorana edge mode predicted to exist in Kitaev quantum spin liquids[2]. However, the temperature and magnetic-field range of the half-quantized signal[2–4] and its association with Majorana edge modes are still under debate[5,6]. Here we present a comprehensive study of the thermal Hall conductivity in α-$RuCl_3$ showing that approximately half-integer quantization exists in an extended region of the phase diagram, particularly across a plateau-like parameter regime for $H_{||}$ exceeding 10 T and temperature below 6.5 K. At lower fields, the thermal Hall conductivity exhibits correlations with complex anomalies in the longitudinal thermal conductivity and magnetization, and is suppressed by cooling to low temperatures. Our results can be explained by the existence of a topological state in magnetic fields above 10 T.

A prime candidate for experimentally accessible quantum spin liquids is the Kitaev model, which has an exactly solvable ground state with itinerant and localized Majorana fermions[7]. Although they are charge-neutral, itinerant Majorana fermions carry heat and are therefore expected to contribute to thermal transport[8]. Applying a magnetic field gaps the bulk Majorana bands, leading to a topologically protected chiral edge current[9]. This edge state carries a thermal Hall conductivity per layer divided by temperature, namely, $k_{XY}{}^{2D}/T = \frac{\pi^2 k_B^2}{6h}$, where k_B and h are the Boltzmann and Planck constants, one-half that of an equivalent electronic edge state in the quantum Hall effect due to the fractionalized nature of the Majorana fermion.

The search for material candidates of the Kitaev model has focused on Mott insulators[10] with $5d^4$ Ir^{4+} and $4d^4$ Ru^{3+} having strong spin–orbit coupling on a honeycomb lattice[11–13]. Here α-$RuCl_3$ is a prime candidate that shows antiferromagnetic zigzag order below the antiferromagnetic ordering temperature $T_N \approx 7.5$ K. This magnetic order is suppressed with an in-plane critical magnetic field of $H_{C2} \approx 7$ T (refs. [2,14–21]), where the magnetic moment is not yet fully saturated, revealing a region of the phase diagram where a quantum spin liquid may arise. A thermal Hall effect with a magnitude close to the half-quantized value k_{HQ}/T (corresponding to $k_{XY}{}^{2D}/T$ per atomic plane) was reported in the quantum spin liquid region with an in-plane magnetic field $H_{||}$ along the a axis (perpendicular to the Ru–Ru bond direction)[2–4], which was discussed as a signature of the Majorana edge state expected for the Kitaev quantum spin liquid.

To establish the presence of an edge state, however, the robustness of the half-quantized thermal Hall effect should be demonstrated over a reasonably wide range of magnetic fields and temperatures. Several studies report a plateau-like region in a field at around 5 K with a magnitude close to k_{HQ}/T (refs. [2–4]). These studies, however, are limited down to ~3.5 K and the plateau behaviour as a function of T is not as clear as it is in the field. The plateau-onset fields differ between studies, ranging from $H_{||} = 7.8$ T (ref. [2]) to 9.9 T (ref. [3]). In preparing this manuscript, we noticed that another study[22] reported a broad k_{XY}/T dome with a height appreciably smaller than k_{HQ}/T, which was interpreted as not supporting the existence of a half-quantized plateau. Recently, anomalies in the magnetocaloric effect, specific heat and magnetic Grüneisen parameter were reported at around $H_{||} = 10$ T (refs. [23–25]) in the spin liquid region (above H_{C2}), suggesting that the phase diagram may be even more complex. The question of the relationship between these anomalies and the thermal Hall signature may be of fundamental importance to understand the nature of the possible field-induced quantum spin liquid, and more specifically, the possible topological edge state.

Here we present comprehensive measurements of k_{XY}, k_{XX} and the magnetic susceptibility (dM/dH) in a T range from 150 mK to 9 K and $H_{||}$ up to 13 T ($H_{||}$ along the a axis) on an α-$RuCl_3$ single crystal, which reveals that k_{XY}/T stays close to k_{HQ}/T over a reasonably wide range of both temperature and magnetic field (below $T = 6.5$ K and from $H_{||} \approx 10$ T up to at least 13 T), hinting at the presence of a protected half-quantized plateau. Below ~10 T, no signature of a plateau is observed and k_{XY}/T is suppressed to zero on lowering the temperature below 6.5 K, which appears to correlate with the multiple high-field ($H_{||} > H_{C2}$) anomalies present in both k_{XX} and dM/dH.

Magnetic-field-induced anomalies in thermal conductivity k_{XX}. The temperature dependence of k_{XX} reproduces the data from previous reports[2] very well and displays a sharp minimum at $T_N = 7.5$ K, which moves to lower temperatures as $H_{||}$ increases and eventually fades out above $H_{C2} = 7.1$ T, tracing the extent of the antiferromagnetically ordered region (Fig. 1a,e). As a function of $H_{||}$, the magnitude of k_{XX} first decreases to a broad minimum at around 7 T and then rapidly increases (Fig. 1b). The data below 2 K reveal additional features in $k_{XX}(H_{||})$: the broad minimum splits into two at $H_{C1} = 6.05$ T and $H_{C2} = 7.10$ T. These fields coincide with two sharp peaks in dM/dH (Fig. 1c), which correspond to two reported transitions: from zigzag-ordered phase I to intermediate-ordered phase II and from phase II to the high-field paramagnetic phase[23–28]. The suppression of k_{XX} at the magnetic-phase transitions is consistent with the interpretation that k_{XX} is dominated by phonons that scatter off magnetic excitations[29].

At higher in-plane magnetic fields and below 5 K, further anomalies can be seen in k_{XX}, namely, a broad maximum at $H_P \approx 10$ T

[1]Max Planck Institute for Solid State Research, Stuttgart, Germany. [2]Department of Physics, Tokyo Institute of Technology, Tokyo, Japan. [3]Department of Physics, The University of Tokyo, Bunkyo, Japan. ✉e-mail: j.bruin@fkf.mpg.de; h.takagi@fkf.mpg.de

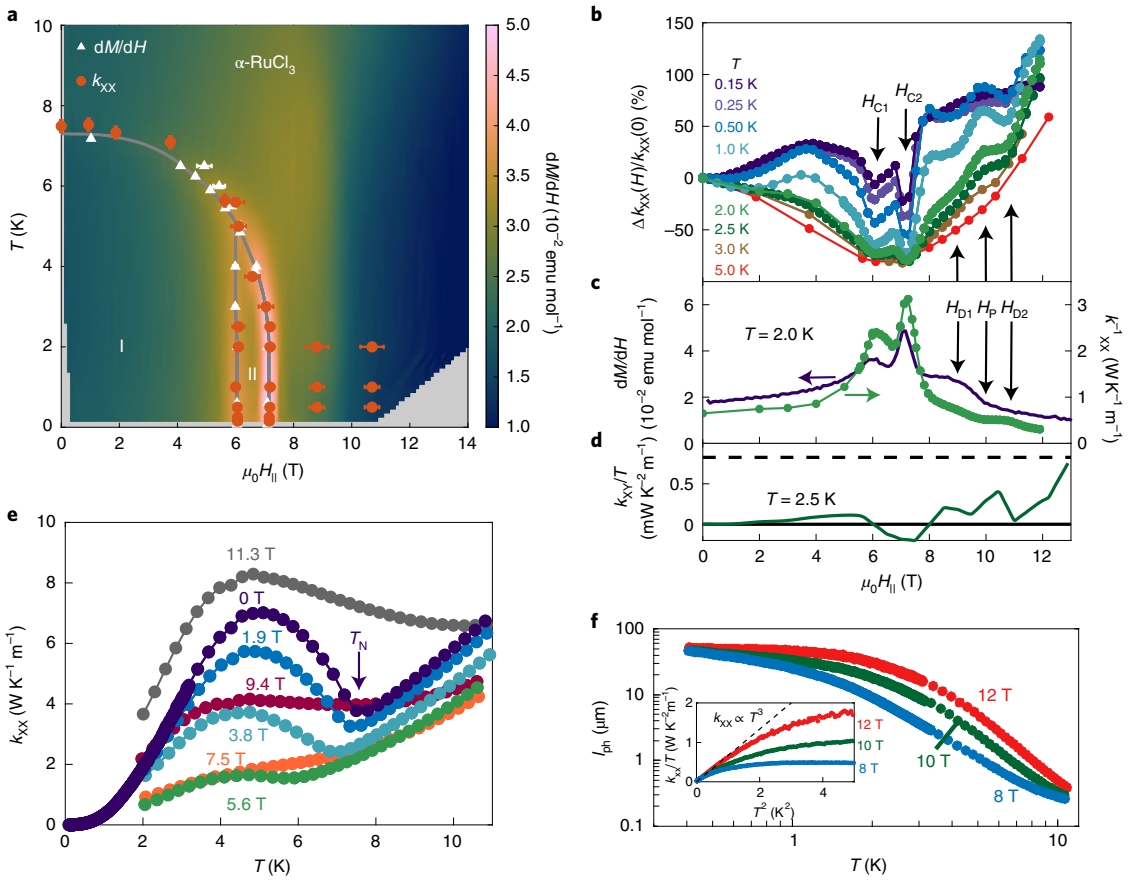

Fig. 1 | Anomalies of thermal conductivity k_{XX} in magnetic field and phase diagram. a, $H_{||}$–T phase diagram of α-$RuCl_3$ derived from features in thermal conductivity (k_{XX}) and magnetic susceptibility (dM/dH). μ_0 is the vacuum permeability. Phases I and II were previously identified as regions of long-range antiferromagnetic order (enclosed by the solid grey lines). The colour plot shows the interpolated magnitude of dM/dH (the raw data are shown in Extended Data Fig. 1). The white triangles mark the local maxima in dM/dH and dM/dT, and the orange points mark the minima in k_{XX}. The error bars represent one standard deviation. **b**, Isotherms of the relative change in k_{XX} with respect to the zero-field value as a function of the magnetic field. Antiferromagnetic transitions H_{C1} and H_{C2}, as well as the features at H_{D1} and H_{D2}, appear as the local minima of k_{XX}; the feature at H_P appears as a broad local maximum. **c**, Comparison of the sequence of anomalies in dM/dH and k_{XX}^{-1} as a function of the magnetic field at 2.0 K. **d**, Thermal Hall conductivity divided by temperature (k_{XY}/T) as a function of the magnetic field at 2.5 K. The data are interpolated from the dataset shown in Fig. 4, and the dashed line is the half-quantized value k_{HQ}/T. **e**, k_{XX} as a function of temperature measured in a ^{4}He-flow cryostat, for in-plane field values ranging from 0 T to 11.3 T. For 0 T, a low-temperature dilution refrigerator measurement is superimposed. The antiferromagnetic transition temperature T_N is identified as a sharp minimum. **f**, Calculated phonon mean free path as a function of temperature. At 12 T, the lowest-temperature phonon mean free path saturates at around 50 μm. Inset: k_{XX}/T at high fields, demonstrating a low-temperature tendency to phonon-driven $k_{XX} \propto T^3$ behaviour (the dashed line is a guide to the eye).

flanked by broad minima at $H_{D1} \approx 8.8$ T and $H_{D2} \approx 10.7$ T (Fig. 1b). Features corresponding to H_{D1} and H_P can be clearly identified as a broad shoulder and a sudden drop in dM/dH, respectively (Fig. 1c and Extended Data Fig. 1). We argue that these high-field anomalies in k_{XX} arise from crossovers or very weak phase transitions.

In analogy to the minima in k_{XX} at H_{C1} and H_{C2}, increased phonon scattering by soft magnetic excitations can explain the minima at H_{D1} and H_{D2}. However, the anomalies at H_{D1} and H_{D2} appear broader and weaker than those at the well-defined phase transitions at H_{C1} and H_{C2} (Fig. 1b). They are enhanced on cooling to 500 mK but subsequently suppressed below 500 mK, indicative of a reduction in phonon scatterers. This suggests that H_{D1} and H_{D2} may not be well-defined phase transitions like H_{C1} and H_{C2} but highly probable crossovers with soft but finite energy excitations or alternatively very weak transitions having only a limited number of low-energy excitations involved.

Recent reports of the magnetocaloric effect[23] and the magnetic Grüneisen parameter[25] at temperatures above 1 K also showed anomalies near H_{D1} and H_{D2}, whereas the specific heat[24] at 0.67 K reported a symmetry-breaking phase transition near 10 T, a conclusion that is contested by several other measurements[23,25,27,28]. In the course of preparing this manuscript, we noticed another work[22] in which broadly similar field-dependent structures are reported in k_{XX} that are ascribed to quantum oscillations from underlying quasiparticles. That scenario, however, does not explain the disappearance of features in the low-temperature limit instead of the expected Lifshitz–Kosevitch behaviour (Extended Data Fig. 2) or the alignment of prominent minima with the well-established magnetic-phase transitions at H_{C1} and H_{C2}.

Thermal Hall conductivity close to the half-quantized value. A strong k_{XY}/T signal is resolved above $H_{C2} = 7.1$ T, as measured by sweeping the temperature at a fixed field (Fig. 2, T sweeps) and a magnetic field at a fixed temperature (Fig. 3, H sweeps). Great care was taken to avoid systematic errors by verifying the linear power dependence of the signal and by avoiding field hysteretic effects that may mix k_{XX} and k_{XY} (Extended Data Figs. 3 and 4 and Supplementary Discussion). Data from H and T sweeps are indeed

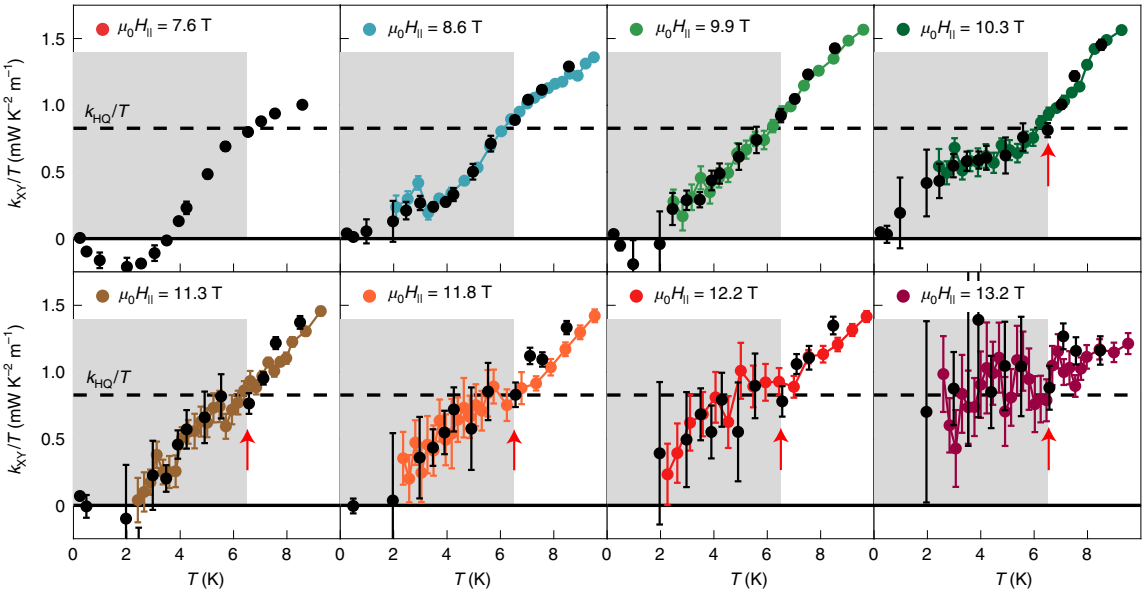

Fig. 2 | Temperature dependence of thermal Hall effect k_{XY}/T. Temperature-dependent k_{XY}/T data in order of increasing in-plane magnetic field from 7.6 T (top left) to 13.2 T (bottom right). The independent results of temperature sweeps at a fixed field (coloured points) and field sweeps at a fixed temperature (black points) are plotted together to demonstrate the high degree of consistency. From 10.3 T onwards, a kink is visible at around 6.5 K (red arrows); beyond this field, the low-temperature magnitude of k_{XY}/T is gradually enhanced towards the half-quantized value k_{HQ}/T (dashed line). The grey-shaded areas emphasize the temperature range below 6.5 K. The error bars represent one standard deviation.

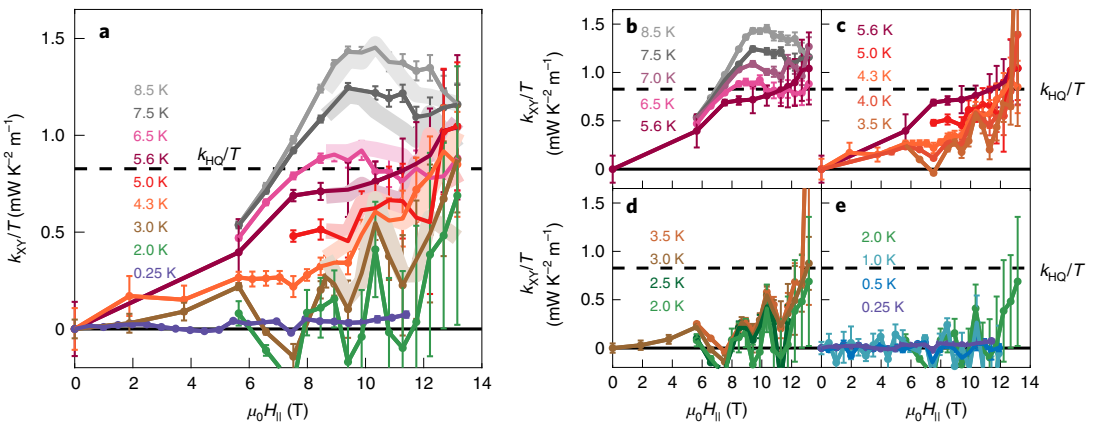

Fig. 3 | Magnetic-field dependence of thermal Hall effect k_{XY}/T. a, Selection of k_{XY}/T isotherms as a function of in-plane magnetic field from 250 mK to 8.5 K. A strong, complex dependence on T and $H_{||}$ is observed, including enhancement at the highest fields towards the half-quantized value k_{HQ}/T (dashed line), suppression on cooling at lower fields and non-monotonic structure for $0.25 < T < 4$ K. The broad shaded lines indicate trends in the interpolated temperature sweeps at a fixed field (Fig. 2) to demonstrate consistency. **b**–**e**, Extended selection of k_{XY}/T isotherms in order of decreasing temperature: 5.6–8.5 K (**b**), 3.5–5.6 K (**c**), 2.0–3.5 K (**d**) and 0.25–2.0 K (**e**). The error bars represent one standard deviation.

consistent with each other within the given error bars, which arise from random noise in thermometry (Fig. 2, black points, and Fig. 3, thick lines). Repeated measurements were performed over multiple months to eliminate the possibility of dependence on contact geometry or sample aging and produce a fully consistent dataset.

As shown in Figs. 2 and 3, k_{XY}/T is larger than the half-quantized value $k_{HQ}/T = 0.87$ mW K^{-2} m^{-1} at high temperatures and at high magnetic fields (above $T = 6.5$ K and $H_{C2} = 7.1$ T) and decreases to k_{HQ}/T and below by lowering T and $H_{||}$, giving rise to a region with $k_{XY}/T \approx k_{HQ}/T$ on the $H_{||}$–T plane. A colour plot of k_{XY}/T across the whole phase diagram (Fig. 4) combines data from all the H and T sweeps, which maps out the region where k_{XY}/T is within ±20% of k_{HQ}/T (white region). We see an L-shaped white region of $k_{XY}/T \approx k_{HQ}/T$, which first runs vertically from $T = 9.0$ K to $T \approx 6.5$ K at around $H_{||} = 7.6$ T and then continues horizontally from $H_{||} \approx 7.6$ T up to at least $H_{||} \approx 13.2$ T at around 6.5 K. The observation of an almost $H_{||}$-independent $k_{XY}/T \approx k_{HQ}/T$ was also reported in previous studies at a similar temperature. In our data, it starts from a similar field of 7.6 T but extends higher to 13.2 T. As we measured a sample that was also studied elsewhere[2], one may argue that the difference arises from a change in the sample quality and/or an experimental error such as dependence on contact geometry or measurement sequence. Sample degradation is unlikely because of the perfect agreement of k_{XX} with that in the original report and reproducibility across multiple measurements (Extended Data Figs. 5 and 6). We also note that our results are reproducible with

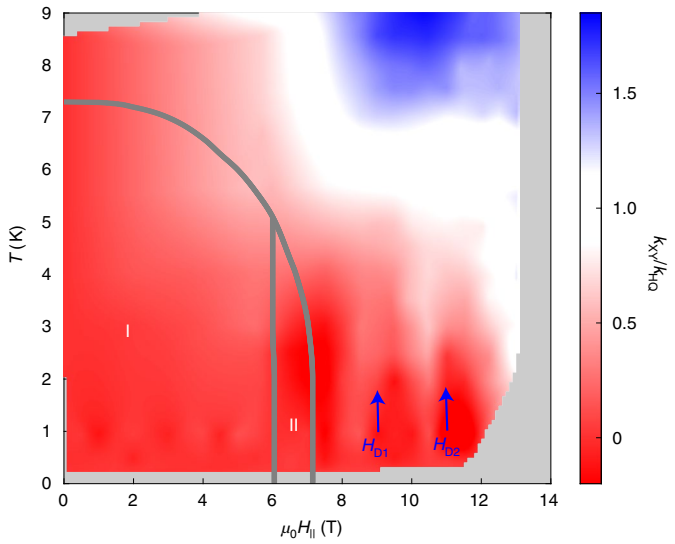

Fig. 4 | Overview of thermal Hall effect k_{XY}/T on the $H_{||}$–T plane. Interpolated magnitude of k_{XY}/T normalized by k_{HQ}/T across the $H_{||}$–T phase diagram. In the colour scheme, white represents a thermal Hall conductivity within 20% of the half-quantized value. The grey lines trace the antiferromagnetic phase transitions (for reference). The two low-temperature minima in k_{XY}/T at H_{D1} and H_{D2} are indicated by arrows.

different sample-mounting geometries (Extended Data Fig. 3) and different sequences of data acquisition (H and T sweeps). Recent studies[3,4] indeed report the region of $k_{XY}/T \approx k_{HQ}/T$ at higher fields than the original study, although the onset field is also higher than the original study and present study. Sample dependence is beyond the scope of this study but should be carefully checked in the future.

The most intriguing feature in Fig. 4 is the notable broadening of the white region at low temperatures with an increasing field above ~10 T, giving rise to a large, triangular white area that extends down to at least 2 K at 13 T. Does the observation of a region with $k_{XY}/T \approx k_{HQ}/T$ on the $H_{||}$–T plane have a physical implication and support the presence of the topologically protected half-quantized plateau? The enhancement of k_{XY}/T could have different origins, for instance, through (non-quantized) topological magnon[5,6] or phonon[30] transport. In such scenarios, a crossing may give rise to an accidental $k_{XY}/T\,(H_{||}, T) \approx k_{HQ}/T$ line on the $H_{||}$–T plane. In contrast, a quantized, topologically protected $k_{XY}/T(H_{||}, T) \approx k_{HQ}/T$ plateau should exhibit insensitivity to changes in both magnetic field and temperature across and in the extended area in $H_{||}$ and T.

The extended nature of $k_{XY}/T\,(H_{||}, T) \approx k_{HQ}/T$ above 10 T represented by the white triangular plane in Fig. 4 argues against an accidental crossing scenario and hints at a half-quantized plateau and hence a Majorana edge state in α-$RuCl_3$. The corresponding T-sweep data (Fig. 2) shows that for fields greater than 10.3 T, a kink-like singularity in the T dependence of k_{XY}/T appears at ~6.5 K (Fig. 2, red arrows). Notably, at the kink, k_{XY}/T is always ~k_{HQ}/T, implying that the magnitude of k_{HQ}/T has special importance in the system. On lowering T, the kink is followed by an almost T-independent $k_{XY}/T \approx k_{HQ}/T$ region, reminiscent of an incipient half-quantized T plateau and then by a rapid decrease to zero. The width of the T-plateau-like region gradually expands on increasing the field from 10.3 T, giving rise to the white triangle in Fig. 4.

The narrow L-shaped white region below $H_{||} \approx 10$ T (Fig. 4), on the other hand, represents a 'line' of $k_{XY}/T\,(H_{||}, T) \approx k_{HQ}/T$, which is clearly demonstrated by the T and H sweeps in Figs. 2 and 3. Along the vertical white region in Fig. 4, k_{XY}/T is smoothly suppressed on cooling at 7.6 T (Fig. 2) and continuously decreases through k_{HQ}/T with decreasing $H_{||}$ in the H sweeps (Fig. 3). Along the horizontal white region at around 6.5 K, k_{XY}/T shows a plateau in the H sweep at 6.5 K (Fig. 3), but continuously decreases through k_{HQ}/T in the T sweeps up to ~10 T. It is not obvious why k_{XY}/T crosses k_{HQ}/T at a constant temperature of 6.5 K. Nevertheless, because of the line character of the region of $k_{XY}/T\,(H_{||}, T) \approx k_{HQ}/T$, the white region (Fig. 4) below $H_{||} \approx 10$ T is probably due to accidental crossing.

Low-temperature suppression of k_{XY}/T. What is the origin of the rapid suppression of k_{XY}/T to zero at low temperatures below 12 T (Fig. 4, red-coloured region)? Within this red region, weak structures are observed: three vertical streaks of minima (deeper red) at around $H_{||} = 7.0$, 9.5 and 11.0 T and two vertical streaks of maxima (brighter red) at around $H_{||} = 8.5$ and 10.0 T branching out from the white region at $T = 6.5$ K. As shown in Figs. 1d and 4, the fields of the three minima apparently coincide with the critical field H_{C2} and the two high-field anomalies at H_{D1} and H_{D2} observed in k_{XX} and dM/dH. The maximum at ~10 T reflects the singularly weak T dependence of k_{XY}/T at $H_{||} = 10.3$ T (Fig. 2) and coincides with H_P. These correlations suggest that the high-field magnetic crossovers/transitions are related to the suppression of k_{XY}/T at low temperatures.

If a half-quantized thermal Hall plateau arises from a chiral Majorana edge mode[8], it was theoretically shown that the coupling between a phonon bath and the edge mode[31,32] is necessary to observe the plateau in the presence of dominant phonon conductivity. Phonons must be in the diffuse rather than the ballistic scattering regime. If phonons experience a crossover from the diffuse to the ballistic regimes on cooling or under a magnetic field, the thermal Hall signal from the Majorana edge mode should vanish due to the decoupling of phonons and edge modes, which might account for the low-temperature suppression of k_{XY}/T. From the estimation of the phonon mean free path (l_{ph}) from k_{XX} as a function of $H_{||}$ and T, however, we may exclude the phonon–edge mode decoupling scenario as the origin of low-temperature suppression of k_{XY}/T below k_{HQ}/T from 7 to 12 T.

k_{XX} approaches a T^3 power law at the highest fields and lowest temperatures (Fig. 1f), consistent with phonon transport limited by a temperature-independent scattering length. The calculated l_{ph} reaches ~50 μm at the lowest temperatures, which is somewhat smaller than the sample width of ~1 mm (Fig. 1f and Extended Data Fig. 7), meaning that phonon transport at low temperatures is still marginally in the diffuse regime. Furthermore, the fact that the regions of suppressed k_{XY}/T coincide with the minima in k_{XX}, that is, regions with the shortest l_{ph}, argues against the decoupling scenario. The low-temperature enhancement of k_{XY}/T to k_{HQ}/T on increasing the magnetic field is accompanied by an increase in l_{ph}, the opposite of what would be expected from phonon–edge mode decoupling. We also note that the decoupling scenario appears to be contrary to a report in which the half-quantized plateau is only observed in samples with high (phonon) thermal conductivity[4].

Recently, the scenario of purely phonon-driven thermal Hall was proposed based on the discovery of a large thermal Hall effect in non-magnetic $SrTiO_3$ and the correlation between the T dependence of k_{XX} and k_{XY} in $RuCl_3$ (ref. [30]). In addition, in the magnetic insulator $Ba_3CuSb_2O_9$, a thermal Hall angle ($\tan(\theta_H) \approx 10^{-4}$), similar to that of $RuCl_3$, was claimed to arise from the phonon thermal Hall effect alone[33]. The observed suppression of k_{XY}/T at low temperatures and its correlation with k_{XX} are in line with a phonon-driven scenario. Both show an overall increase on increasing the field, with dip-like suppressions at H_{D1} and H_{D2}. Although a phonon-only scenario could explain these correlations between k_{XX} and k_{XY}, it is not clear how it would naturally explain the observed plateau-like behaviour of k_{XY}/T close to k_{HQ}/T.

The identification of possible topological phase transitions into and out of the half-quantized state still remains an open question[23–25,27,28]. For the former, unveiling the nature of high-field

anomalies may be the key question to be addressed. The high-field transition out of the half-quantized state, if it exists, must be at a field higher than 13 T. A measurement of k_{XY}/T to much higher fields is, therefore, highly desired. Alternative mechanisms leading to an enhancement of k_{XY}/T, such as a topological magnon-driven[5,6] or phonon-driven[30] Hall effect, have been proposed. Our results do not exclude those scenarios but pose them a challenge to explain the plateau-like behaviour close to half-quantization.

Online content

Any methods, additional references, Nature Research reporting summaries, source data, extended data, supplementary information, acknowledgements, peer review information; details of author contributions and competing interests; and statements of data and code availability are available at https://doi.org/10.1038/s41567-021-01501-y.

Received: 25 April 2021; Accepted: 22 December 2021;
Published online: 17 February 2022

References

1. Balents, L. Spin liquids in frustrated magnets. *Nature* **464**, 199–208 (2010).
2. Kasahara, Y. et al. Majorana quantization and half-integer thermal quantum Hall effect in a Kitaev spin liquid. *Nature* **559**, 227–231 (2018).
3. Yokoi, T. et al. Half-integer quantized anomalous thermal Hall effect in the Kitaev material candidate α-$RuCl_3$. *Science* **373**, 568–572 (2021).
4. Yamashita, M., Kurita, N. & Tanaka, H. Sample dependence of the half-integer quantized thermal Hall effect in a Kitaev candidate α-$RuCl_3$. *Phys. Rev. B* **102**, 220404 (2020).
5. McClarty, P. A. et al. Topological magnons in Kitaev magnets at high fields. *Phys. Rev. B* **98**, 060404 (2018).
6. Zhang, E. Z., Chern, L. E. & Kim, Y. B. Topological magnons for thermal Hall transport in frustrated magnets with bond-dependent interactions. *Phys. Rev. B* **103**, 174402 (2021).
7. Kitaev, A. Anyons in an exactly solved model and beyond. *Ann. Phys.* **321**, 2–111 (2006).
8. Nasu, J., Yoshitake, J. & Motome, Y. Thermal transport in the Kitaev model. *Phys. Rev. Lett.* **119**, 127204 (2017).
9. Motome, Y. & Nasu, J. Hunting Majorana fermions in Kitaev magnets. *J. Phys. Soc. Jpn* **89**, 012002 (2020).
10. Jackeli, G. & Khaliullin, G. Mott insulators in the strong spin-orbit coupling limit: from Heisenberg to a quantum compass and Kitaev models. *Phys. Rev. Lett.* **102**, 017205 (2009).
11. Trebst, S. & Hickey, C. Kitaev materials. *Phys. Rep.* **950**, 1–37 (2022).
12. Winter, S. M., Li, Y., Jeschke, H. O. & Valentí, R. Challenges in design of Kitaev materials: magnetic interactions from competing energy scales. *Phys. Rev. B* **93**, 214431 (2016).
13. Takagi, H., Takayama, T., Jackeli, G., Khaliullin, G. & Nagler, S. E. Concept and realization of Kitaev quantum spin liquids. *Nat. Rev. Phys.* **1**, 264–280 (2019).
14. Baek, S. H. et al. Evidence for a field-induced quantum spin liquid in α-$RuCl_3$. *Phys. Rev. Lett.* **119**, 037201 (2017).
15. Wang, Z. et al. Magnetic excitations and continuum of a possibly field-induced quantum spin liquid in α-$RuCl_3$. *Phys. Rev. Lett.* **119**, 227202 (2017).
16. Zheng, J. et al. Gapless spin excitations in the field-induced quantum spin liquid phase of α-$RuCl_3$. *Phys. Rev. Lett.* **119**, 227208 (2017).
17. Banerjee, A. et al. Excitations in the field-induced quantum spin liquid state of α-$RuCl_3$. *npj Quant. Mater.* **3**, 8 (2018).
18. Johnson, R. D. et al. Monoclinic crystal structure of α-$RuCl_3$ and the zigzag antiferromagnetic ground state. *Phys. Rev.* **92**, 235119 (2015).
19. Kubota, Y., Tanaka, H., Ono, T., Narumi, Y. & Kindo, K. Successive magnetic phase transitions in α-$RuCl_3$: XY-like frustrated magnet on the honeycomb lattice. *Phys. Rev. B* **91**, 094422 (2015).
20. Yadav, R. et al. Kitaev exchange and field-induced quantum spin-liquid states in honeycomb α-$RuCl_3$. *Sci. Rep.* **6**, 37925 (2016).
21. Sears, J. A. et al. Magnetic order in α-$RuCl_3$: a honeycomb-lattice quantum magnet with strong spin-orbit coupling. *Phys. Rev. B* **91**, 144420 (2015).
22. Czajka, P. et al. Oscillations of the thermal conductivity observed in the spin-liquid state of α-$RuCl_3$. *Nat. Phys.* **17**, 915–919 (2021).
23. Balz, C. et al. Finite field regime for a quantum spin liquid in α-$RuCl_3$. *Phys. Rev. B* **100**, 60405 (2019).
24. Tanaka, O. et al. Thermodynamic evidence for field-angle dependent Majorana gap in a Kitaev spin liquid. Preprint at https://arxiv.org/abs/2007.06757v1 (2020).
25. Bachus, S. et al. Thermodynamic perspective on field-induced behavior of α-$RuCl_3$. *Phys. Rev. Lett.* **125**, 97203 (2020).
26. Balz, C. et al. Field-induced intermediate ordered phase and anisotropic interlayer interactions in α-$RuCl_3$. *Phys. Rev. B* **103**, 174417 (2021).
27. Ponomaryov, A. N. et al. Nature of magnetic excitations in the high-field phase of α-$RuCl_3$. *Phys. Rev. Lett.* **125**, 37202 (2020).
28. Schönemann, R. et al. Thermal and magnetoelastic properties of α-$RuCl_3$ in the field-induced low-temperature states. *Phys. Rev. B* **102**, 214432 (2020).
29. Hentrich, R. et al. Unusual phonon heat transport in α-$RuCl_3$: strong spin-phonon scattering and field-induced spin gap. *Phys. Rev. Lett.* **120**, 117204 (2018).
30. Li, X., Fauqué, B., Zhu, Z. & Behnia, K. Phonon thermal Hall effect in strontium titanate. *Phys. Rev. Lett.* **124**, 105901 (2020).
31. Vinkler-Aviv, Y. & Rosch, A. Approximately quantized thermal Hall effect of chiral liquids coupled to phonons. *Phys. Rev. X* **8**, 31032 (2018).
32. Ye, M., Halász, G. B., Savary, L. & Balents, L. Quantization of the thermal Hall conductivity at small Hall angles. *Phys. Rev. Lett.* **121**, 147201 (2018).
33. Sugii, K. et al. Thermal Hall effect in a phonon-glass $Ba_3CuSb_2O_9$. *Phys. Rev. Lett.* **118**, 145902 (2017).

Methods

Samples. Large, thin (~2.5 mm × 1.3 mm × 17 μm), high-quality single crystals of α-$RuCl_3$ from the same growth batches as those reported in ref. [2] were measured. The sample under investigation for thermal Hall measurements has a confirmed half-quantized Hall plateau in that report, where it was labelled as 'sample 2'. A second sample with a similarly high thermal conductivity was used for magnetic susceptibility measurements.

Thermal conductivity was measured using a steady-state three-thermometer setup. For the temperature range of 1.8–9.0 K, Cernox CX-1050 chip thermometers (Lake Shore) were used in a ^{4}He cryostat. For the temperature range of 150 mK to 3 K, ruthenium oxide chip thermometers were used in a dilution fridge. In each case, thermometers were calibrated in situ against a field-calibrated reference thermometer. A 10 kΩ NiCr resistive heater was used to apply heater power. The sample was free standing with its 'cold' edge mounted with Apiezon N grease onto a LiF single crystal, which was attached with silver paint onto a copper mount and cooled by the cryostat. Several copper mounts machined at different angles were used to allow for measurements in fixed tilted fields.

Geometrical error affects the measurement due to the finite contact sizes and uncertainty in determining the exact crystal dimensions. We estimate the resulting systematic uncertainty in k_{xy}/T to be around 10%, which is in addition to the random error due to thermometry noise (error bars shown in Figs. 2 and 3).

We adopt the usual convention that the crystal a axis is perpendicular to Ru–Ru bonds, the b axis lies along the Ru–Ru bonds and the c axis is perpendicular to the honeycomb plane. The magnetic field was applied at either 70° from the c axis (^{4}He) or 90° from the c axis (dilution refrigerator), with the in-plane field component in the a axis. The amplitude of k_{xx}, as well as the measured transition fields (H_{c1}, H_{c2}, H_{D1} and H_{D2}), were confirmed to reproduce at the same values of $H_{||}$ for these two field angles (Extended Data Fig. 6); therefore, the two datasets are presented as one. The field angle was determined under an optical microscope with 1° precision. Heat was always applied along the a axis.

Over the course of these measurements, the crystal was thermally cycled between room temperature and <4.2 K for 14 times; each time, identical values of k_{xx} were measured, indicating that sample deterioration over time is negligible. The measurement of k_{xx} is additionally in very close agreement with that previously measured in Kyoto (Extended Data Fig. 5).

Magnetization measurements above 2 K were performed using a Physical Property Measurement System vibrating sample magnetometry option (Quantum Design), and below 1 K using a custom-built Faraday force magnetometer on a dilution refrigerator (Extended Data Fig. 1). For all the magnetization data, the applied field was parallel to the crystal a axis.

Data availability

The data that support the findings of this study are available from the corresponding authors upon reasonable request. Source data are provided with this paper.

Acknowledgements

We thank Y. Kasahara and Y. Matsuda for insightful discussions and M. Dueller and K. Pflaum for technical assistance. The work done in Germany has been supported in part by the Alexander von Humboldt Foundation. H. Tanaka and N.K. have been supported by JSPS KAKENHI via grant nos. JP17H01142 and JP19K03711, respectively. H. Takagi has been supported in part by JSPS KAKENHI via grant no. JP17H01140.

Author contributions

J.A.N.B., R.R.C., Y.M. and H. Takagi conceived the research. N.K. and H. Tanaka synthesized the single crystals. J.A.N.B. and R.R.C. designed and performed the thermal conductivity experiments. Y.M. designed and performed the magnetic susceptibility experiments. J.A.N.B., R.R.C., Y.M. and H. Takagi analysed the data and participated in the writing of the paper. All the authors contributed to the manuscript preparation.

Funding

Open access funding provided by Max Planck Society.

Competing interests

The authors declare no competing interests.

Additional information

Extended data is available for this paper at https://doi.org/10.1038/s41567-021-01501-y.

Supplementary information The online version contains supplementary material available at https://doi.org/10.1038/s41567-021-01501-y.

Correspondence and requests for materials should be addressed to J. A. N. Bruin or H. Takagi.

Peer review information *Nature Physics* thanks David Mandrus and the other, anonymous, reviewer(s) for their contribution to the peer review of this work.

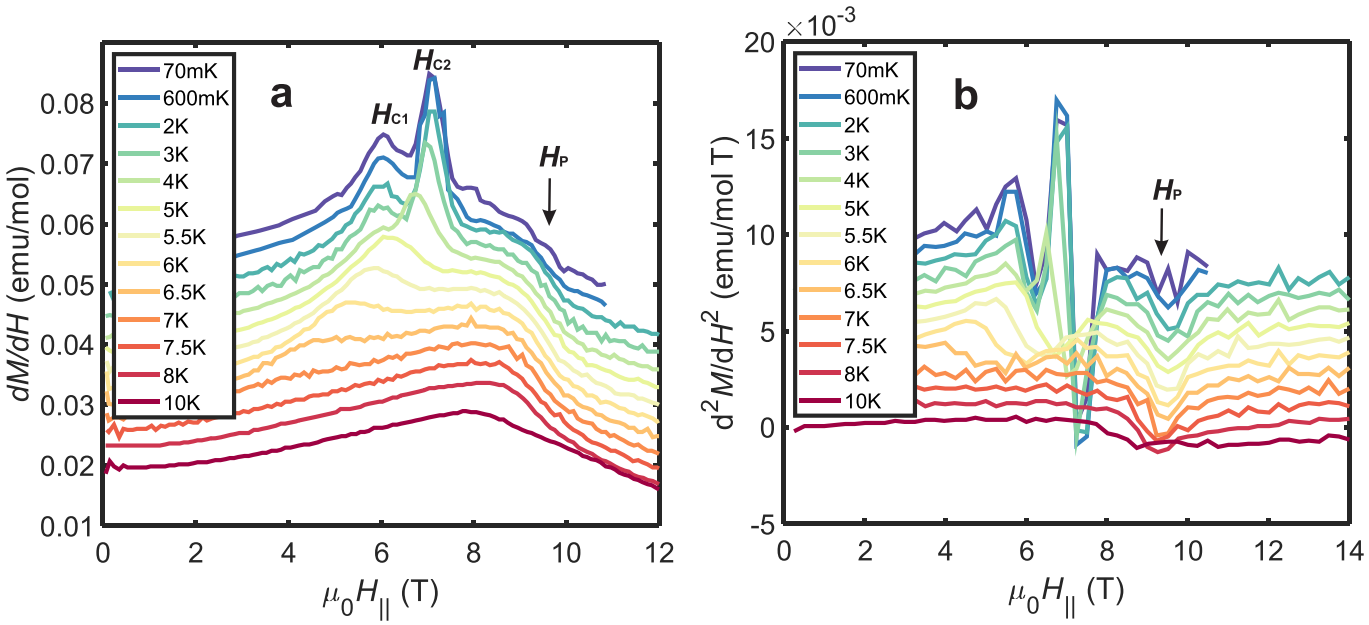

Extended Data Fig. 1 | Magnetization isotherms and phase transitions. Field dependences of d*M*/d*H* which were used to construct the phase diagram in Fig. 1a (main text). **a**, isotherms of d*M*/d*H*, with every curve offset by 0.003 emu/mol for clarity. Phase transitions out of the antiferromagnetic phases H_{C1}, H_{C2} are identified by peaks in d*M*/d*H*, whereas H_P coincides with a drop in d*M*/d*H*. **b**, isotherms of d^2M/dH^2, where the feature at H_P is identified as a local minimum. H_P shifts only minimally in field upon heating, and is no longer resolved at 10 K. Curves are offset by 8×10^{-4} emu/mol T for clarity.

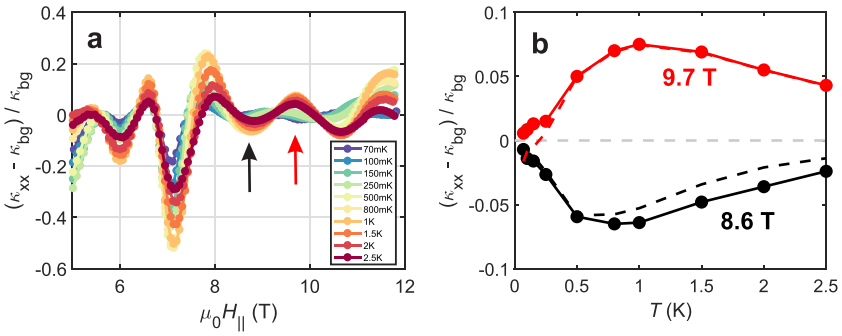

Extended Data Fig. 2 | Temperature dependence of high-field features in k_{xx}. The amplitude of high-field features in k_{XX} is expressed as $(k_{XX} - k_{bg})/k_{bg}$, where k_{bg} is a smooth background fit which passes through the points where k_{XX} has greatest field derivative (as discussed in Ref. [22]). **a**, field dependence $(k_{XX} - k_{bg})/k_{bg}$ for temperatures between 70 mK (dark blue) and 2.5 K (dark red). **b**, temperature dependence of $(k_{XX} - k_{bg})/k_{bg}$ at the local minimum at ~8.6 T and the local maximum at ~9.7 T, indicated by arrows in panel a. The amplitude at constant field (dashed lines), and the amplitudes at the fields of maximum amplitude (solid lines and markers) differ slightly due to a temperature-dependent phase shift. The amplitudes initially increase upon cooling but peak around 1 K and then rapidly collapse to zero down to the lowest measured temperature, in marked contrast to the Lifshitz-Kosevitch behavior expected for conventional quantum oscillations.

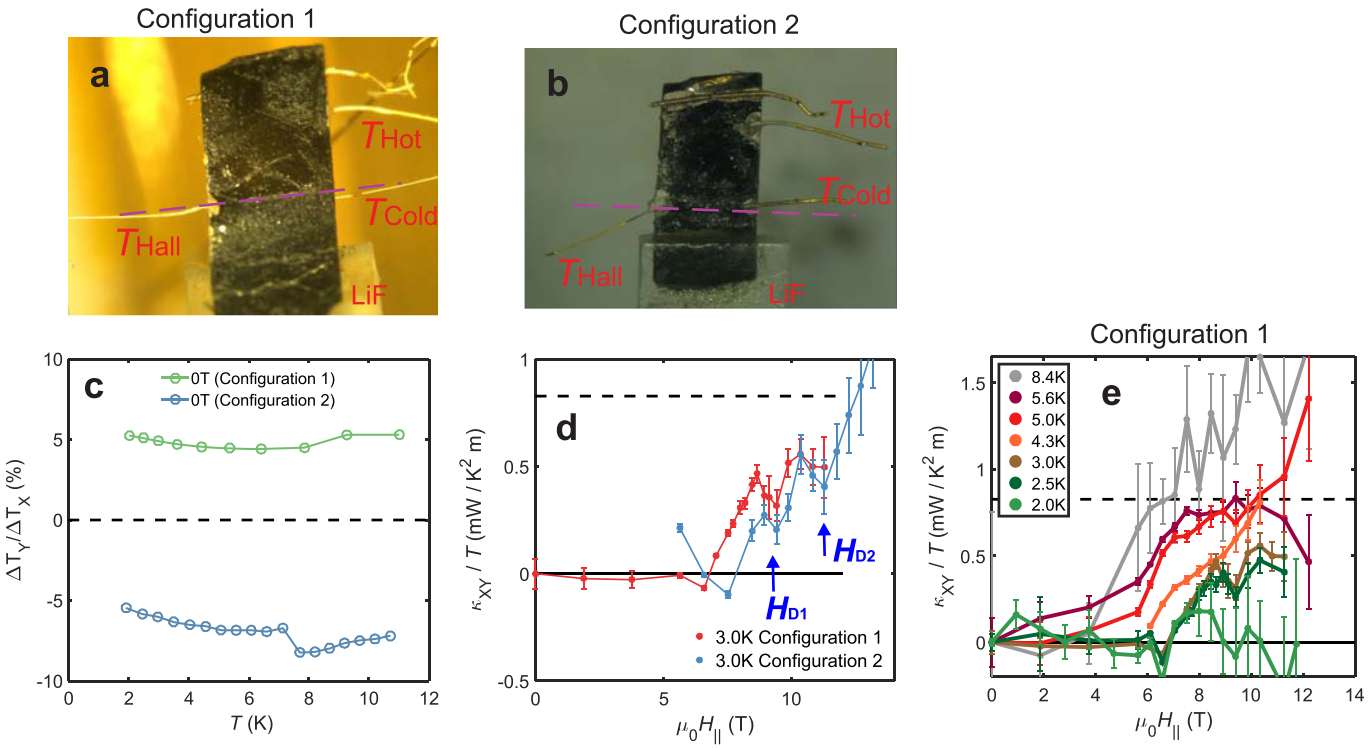

Extended Data Fig. 3 | Excluding error arising from Hall contact offset. a,b, photographs of sample 2 with wires attached in different configurations 1 and 2. The latter configuration was the one used for the measurements shown in the main text. Purple dashed line are guides to the eye to help identify the contact offset. **c**, measured Hall contact offset expressed as $\Delta T_Y/\Delta T_X$ (%) at 0 T, showing the expected inverse offsets for the two configurations. In the absence of an offset, $\Delta T_Y/\Delta T_X$ would be zero (dashed line). **d**, isotherms of k_{XY}/T at 3.0 K for both contact configurations, displaying the same features at H_{D1} and H_{D2}. **e**, isotherms of k_{XY}/T for configuration 1 at multiple temperatures, demonstrating the reproducibility of all the main features observed with configuration 2 (main text, Fig. 3).

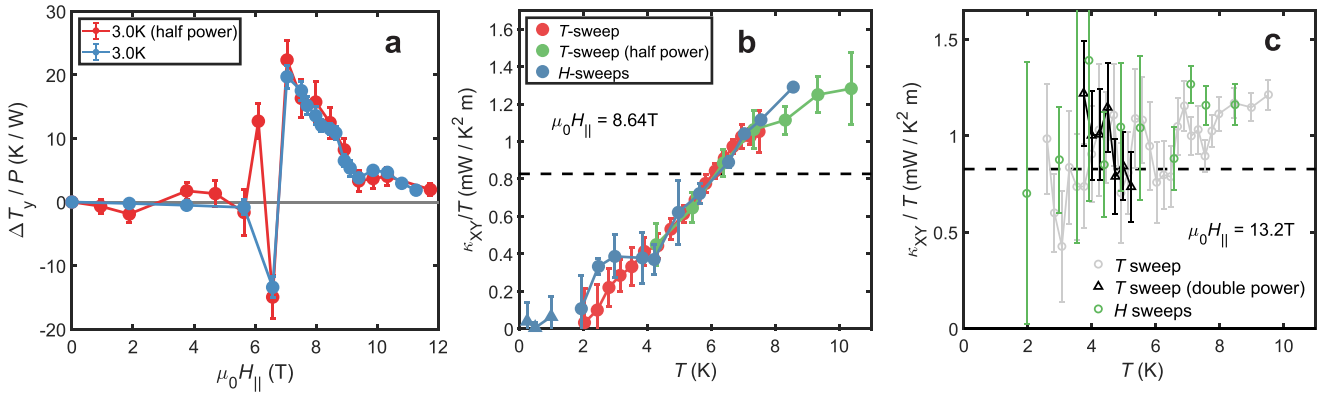

Extended Data Fig. 4 | Excluding power dependence in k_{xy}. Repeated measurements at different levels of heater power demonstrate that the measured thermal conductivity and thermal Hall conductivity are independent of the applied heater power. **a**, Hall temperature gradient normalized by heater power ($\Delta T_y/P$) for two independent isotherms at 3 K, one of which was performed at half the standard heater power (red markers, $\Delta T_x/T \approx 5\%$). The two curves overlap as expected. **b**, the temperature dependence of k_{xy}/T at 8.64 T is compared for two T sweeps, one of which was performed at half power (green markers, $\Delta T_x/T \approx 5\%$), together with full-power H sweeps. All curves overlap within error. **c**, temperature dependence of k_{xy}/T is compared for two T sweeps at 13.2 T, one of which was performed at double the usual power ($\Delta T_x/T \approx 20\%$), together with normal-power H sweeps. The data overlap within the (substantially field-enhanced) error bars.

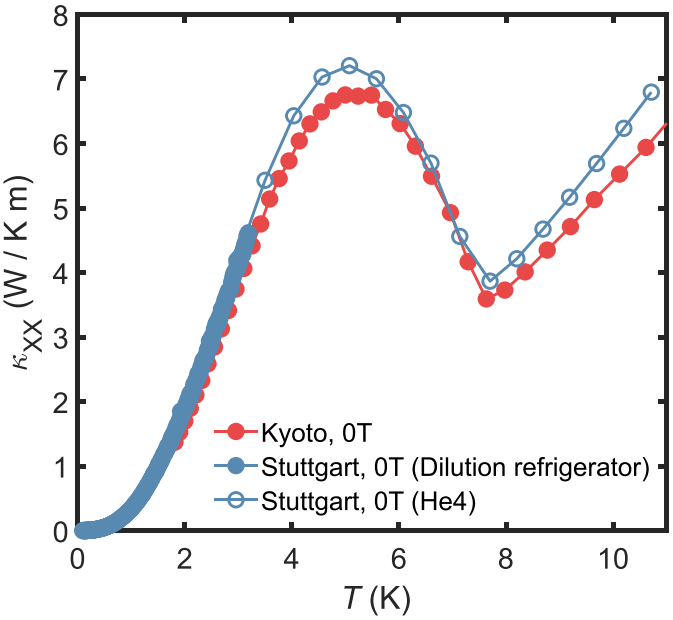

Extended Data Fig. 5 | Reproducibility of thermal conductivity measurements. Comparison of three independent measurements of the thermal conductivity (k_{xx}) of sample 2. Red circles: data measured in Kyoto, Solid blue circles: data taken in a dilution refrigerator in Stuttgart, open blue circles: data taken in a ^{4}He flow cryotstat in Stuttgart. Each measurement had slightly modified contact placements.

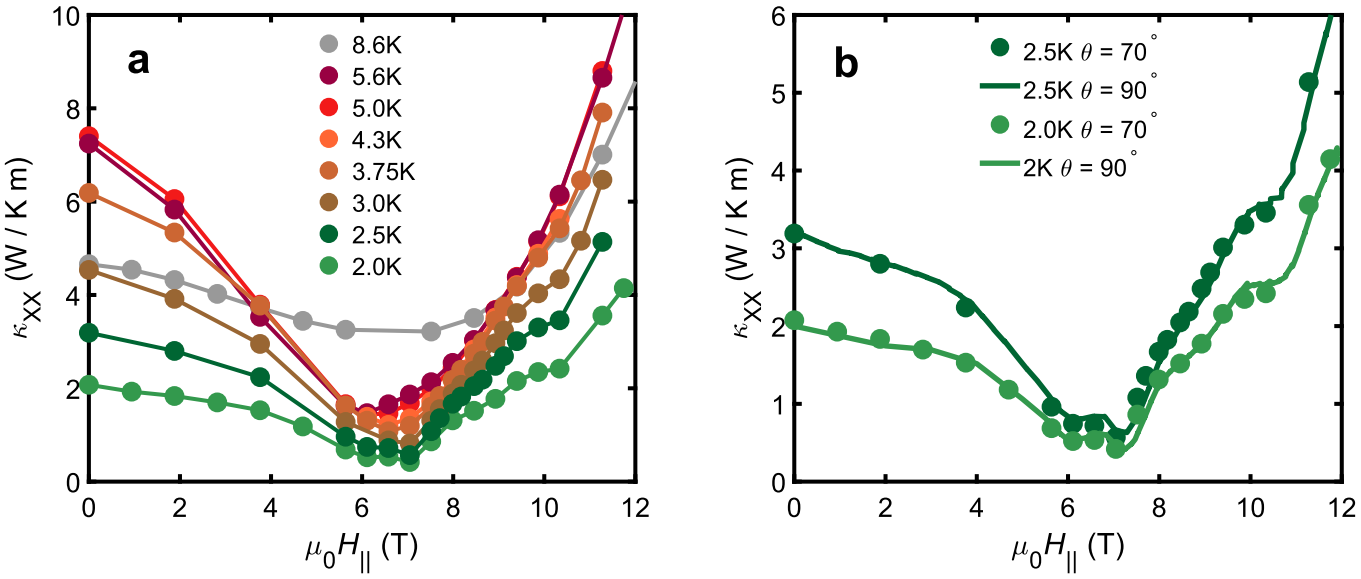

Extended Data Fig. 6 | Temperature and magnetic field-angle dependence of the thermal conductivity above 2.0 K. a, field dependence of k_{XX} up to 12 T for the temperature range 2.0 K – 8.6 K. The sharp features in the field dependence of k_{XX} seen at low temperature rapidly disappear upon heating above 3.0 K. At high temperatures, the field dependence displays a single, broad minimum around 7 T. At 8.6 K, which is above the ordering temperature T_N = 7.5 K, the field dependence is dramatically weakened, although a high field upturn persists at this temperature. **b**, comparison of the field dependence of k_{XX} at 2.0 K and 2.5 K, at field angles of 70° (markers) and 90° (lines) with respect to the *c*-axis. The near-perfect overlap of the data sets demonstrates the insensitivity to magnetic field angle.

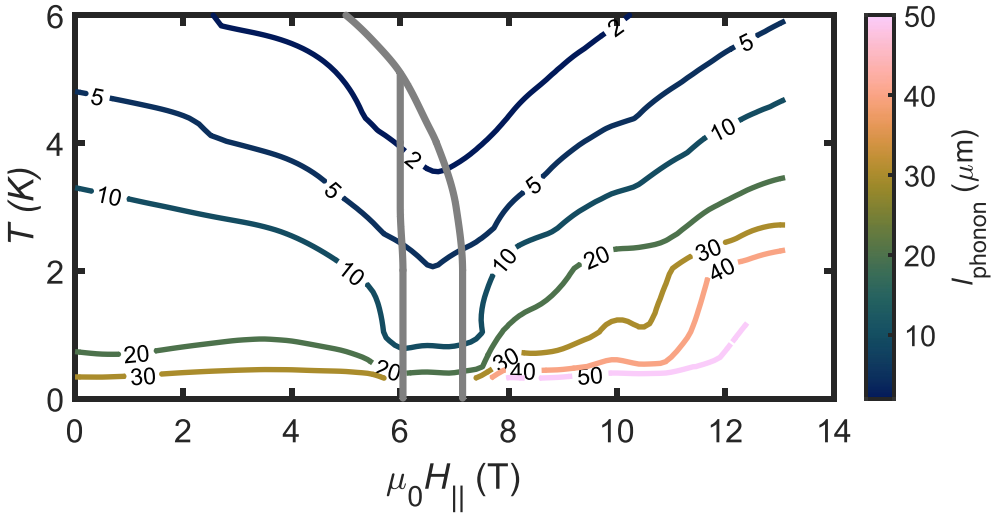

Extended Data Fig. 7 | Calculated phonon mean free path across the $H_{||}$,T phase diagram. Contour plot of the calculated phonon mean free path $l_{ph} = 3\, k_{XX} / C\, v$, where C is the phonon specific heat per unit volume and v is the average phonon velocity. We assume a magnetic field-independent low temperature phonon specific heat with magnitude $C_{ph}/T^3 = 1.22$ mJ mol^{-1}K^{-4} as reported in Ref. [24]. The phonon velocity is estimated using the Debye relation $v = \left(\frac{2\pi^2 k_B^4}{5\beta\hbar^3}\right)^{\frac{1}{3}} \approx 1700 m/s$ where $\beta = C_{ph}/T^3$ as before. The grey lines trace the antiferromagnetic phase transitions, for reference.